Scientific Visualization, 2023, volume 15, number 3, pages 92 - 100, DOI: 10.26583/sv.15.3.10

Heat Fluxes Visualization in High Speed Flow behind the Shock Wave

I.A. Znamenskaya[1,A], M.I. Muratov[2,A], E.A. Karnozova[3,A], A.E. Lutsky[4,B]

[A] Moscow State University, Faculty of Physics, Russia, Moscow,
[B] Keldysh Institute of Applied Mathematics RAS

[1] ORCID: 0000-0001-6362-9496, znamen@phys.msu.ru
[2] ORCID: 0000-0002-6545-5829, muratov583@gmail.com
[3] ORCID: 0000-0001-9611-443X, Liza.Karnozova@yandex.ru
[4] ORCID: 0000-0002-4442-0571, allutsky@yandex.ru

Abstract

The paper presents the thermographic studies of unsteady heat fluxes behind a plane shock wave in the rectangular 24x48 mm shock tube test section. Consecutive panoramic visualization of the heat fluxes plots on streamlined walls after the plane shock wave interaction with a rectangular obstacle fixed on the channel wall are obtained. The duration of the recorded thermal processes is up to 40 milliseconds after the shock wave passage. The heating and cooling of the test chamber walls streamlined by supersonic flow are visualized using the Telops FAST M200 high-speed infrared camera (operating range 1.5 – 5.1 microns) through the quartz windows transparent to infrared radiation. Visualization of the thermal fields were compared with the shadow images and results of 2D numerical simulation of a nonstationary gas dynamic process after the diffraction of a shock wave with Mach numbers M=2.0-4.5.

Keywords: flow visualization, infrared thermography, shock wave diffraction, unsteady heat fluxes, high-speed shadow shooting, numerical simulation.

1 Introduction

The interaction of high-speed gas-dynamic flows with streamlined surfaces has always been a significant problem both in fundamental science and in practical applications. The emerging heat exchange between the gas flow and solid streamlined walls of various geometry in the boundary layers introduces significant changes in the nature of the flow and the state of the gaseous medium [1–3]. The need to analyze complex heat and gas dynamic processes has led to great attention to the various flow visualization methods. The development of digital methods for fast processes in liquids and gases optical visualization has made it possible to increase the range of spatiotemporal parameters of the considered phenomena [4, 5]. Classical visualization methods are: modifications of shadow methods, schlieren methods, as well as interferometry - based on the phenomenon of light deflection when it passes through density inhomogeneities of a transparent medium. These methods are widely used in panoramic visualization of flows with discontinuities [6].

In this paper we used the method of shadow imaging, as well as a rapidly developing non-contact method for studying the thermal radiation - infrared thermography. The key advantage of this technique is the possibility of recording thermal radiation from the heated surface and converting it into a temperature map [7]. The use of infrared thermography in the study of heat flows in a gas-dynamic channel has the advantage of panoramic non-invasive techniques over local measurements [8, 9] due to spatial resolution, and, accordingly, thermal and gas-dynamic processes understanding even when there are great spatial gradients of measured values [10, 11]. Modern infrared thermography makes it possible to

obtain two-dimensional thermal plots (up to 1 MPix), has a high sensitivity to temperature changes (up to 20 mK), and a high recording rate (with exposure time up to 20 μs) [12].

Based on the high-speed infrared thermography, the surfaces thermal fields experimental study is carried out during the shock wave with Mach numbers M = 2.0-4.5 diffraction on a rectangular obstacle located on the lower channel wall and the cocurrent flow behind it. Thermographic and shadow high-speed frame-by-frame visualization of the channel supersonic and transonic flow through quartz side walls of the shock tube test chamber, transparent in the visible and infrared range is implemented.

2 Experimental setup and diagnostics

2.1 Shock tube

The experiments were carried out on a device UTRO-3, a single-diaphragm shock tube with high and low pressure chambers separated by a thin polymer diaphragm. Thickness of the broken diaphragm variation, as well as pressure ratio between the chambers choice, made it possible to set the Mach numbers of the incident shock wave in the range M=2.0–4.5 at an initial air pressure of 5–30 Torr. The incident shock wave velocity was measured by piezoelectric pressure sensors in the low-pressure chamber (Fig. 1 A), separated by a specified distance. The shock wave plane front formation was at a distance of about a meter from the diaphragm. The cocurrent flow velocity behind the shock wave front was estimated in the range of 630–920 m/s. In the test chamber, a sufficiently homogeneous supersonic cocurrent flow with a duration time of up to 500 μs, locked by a contact surface, was realized. The flow Reynolds number, estimated from the width of the shock tube channel, was $Re \sim 10^5$.

A test section is mounted in the low-pressure chamber, which has two side quartz windows transparent in the visible and infrared range (bandwidth 200 - 2800 nm). In the tect chamber, a rectangular obstacle 2 mm × 48 mm × 6 mm in size made of a dielectric material was installed on the bottom wall across the oncoming flow (Fig. 1 D). The high and low pressure chambers length is 52 and 290 cm respectively; the copper walls of the low-pressure chamber thickness is 2 mm; the inner section of the channel of the shock tube and the discharge chamber is 48 × 24 mm; dimensions of two quartz windows - 170 mm × 16 mm × 24 mm. The distance between the piezoelectric sensors was 103 cm. The working and pushing gases were air and helium, respectively. Sensors connected to an oscilloscope (Fig. 1 C) synchronized the of recording thermal imaging equipment or shadow recording with various stages of the gas-dynamic process implemented in the test chamber.

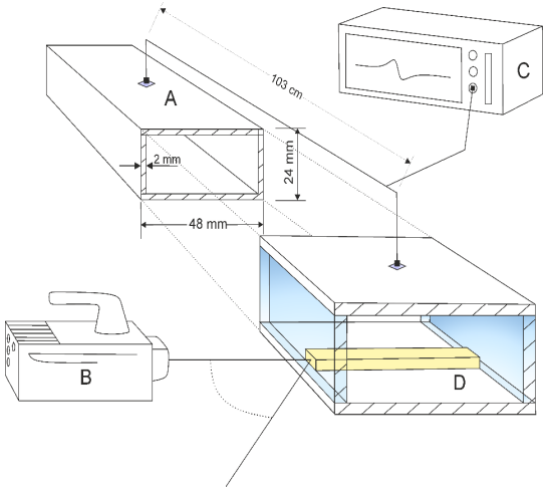

Fig. 1. Experimental setup scheme.

2.2 Shadow visualization

Shadow shooting of the gas-dynamic flow of the high speed flow was carried out using the laser shadow scheme in parallel beams with a high-speed camera. A shadow scheme with a stationary laser as a light source (wavelength 532 nm) was used. The optical beam passed perpendicular to the camera glasses in the area of the stepped obstacle. The optimal shooting speed was 150,000 frames per second with an exposure time 1 microsecond. To improve the quality of shadow images, a program for processing source images with subtraction of the background frame was used.

2.3 Thermographic visualization.

A high–speed, cooled, high-resolution photon detector was used as an infrared radiation receiver (Fig. 1 B): Telops Fast M200 (operating range 1.5 - 5.1 microns). Reducing the spatial resolution of the camera several times allowed the heat fluxes registration at a frequency of up to 2000 frames / s; the integration time ranged from 500 microseconds to 1 ms. The thermal imager was installed at a distance of 25-30 cm from the flow area, while the optical axis of the detector was directed perpendicular to the shock tube main axis; in some experiments, the thermal imager was installed at a certain angle to the tube axis. The heat fluxes measurement was carried out from the surfaces of the obstacle and from the walls of the test chamber heated by the streamlining supersonic and transonic flow.

The diagnostic equipment software is configured to configure the absence of any medium other than the atmosphere between the object and the recorder. Otherwise, the chain of quations for determining the total radiation flux by the detecting device should be supplemented with the terms of the intermediate medium flow. Thus, the presence of a permeable quartz glass on the camera optical axis does not allow us to make quantitative estimates of thermal fields with a given accuracy in this task.

3 Results and discussion

3.1 Plane shock wave diffraction of the ledge

The plane shock wave interaction with an obstacle (ledge) is accompanied by a non-stationary process of its diffraction and reflection (Fig. 2). The reflection of the incident wave front from the windward surface and the flow of a rectangular obstacle by a satellite stream behind the incident shock wave are considered. Diffraction of the passing shock wave occurs in 20-30 microseconds, and then the reflected shock wave slowly moves away from the obstacle towards the flow in times of 300-200 microseconds, depending on the Mach number of the incident wave.

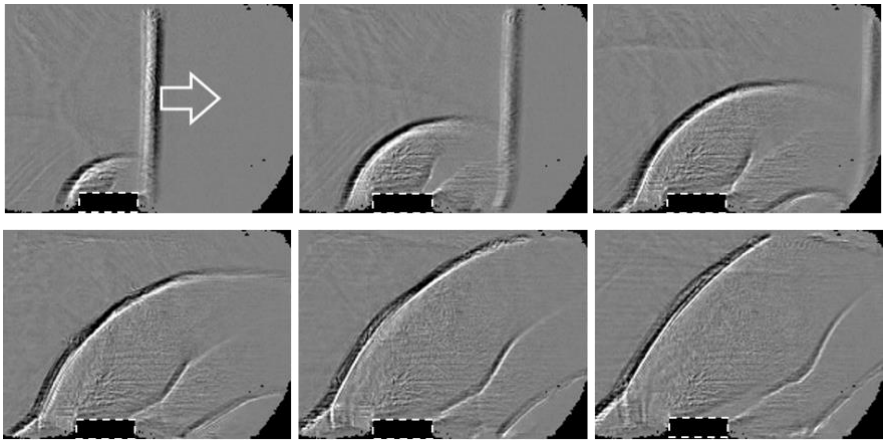

Fig. 2. Frame-by-frame visualization of shock wave diffraction (M = 3.1) made by shadow optical method, F = 150000 frame/s

3.2 Numerical simulation

Numerical simulation of the considered flow was implemented via the usage of the two-dimensional Navier-Stokes equations. The main task of modeling was to study the movement and the evolution of mainstream splits. More subtle effects, such as the interaction of shock waves with boundary layers on the channel walls and obstacles, were excluded. The algorithm [13] is based on the generalized Godunov scheme with piecewise linear TVD reconstruction of gas-dynamic functions in the cells. Inviscid flows on the cell edges were determined based on exact solutions of the Riemann problem on the edges in the projection to the normal. The velocity and the temperature derivatives required for viscous flows were determined using the Green-Gauss formulas. Grid in the region $-0.052 < x < 0.34$; $0 < y < 0.024$ contained 3940×240 cells.

Comparative analysis of the numerical calculation results of gas-dynamic parameters and experimental frames from high-speed imaging (shadow and infrared) showed a visual similarity of the main structural features of the studied flows.

Figure 3 shows two images of shock wave diffraction on an obstacle. The high-velocity flow around the obstacle in the channel is defined by the inhomogeneous density field around the streamlined insert (Fig. 3 right). The area near the windward wall of the obstacle is characterized by a high degree of density and temperature in the zone of flow deceleration.

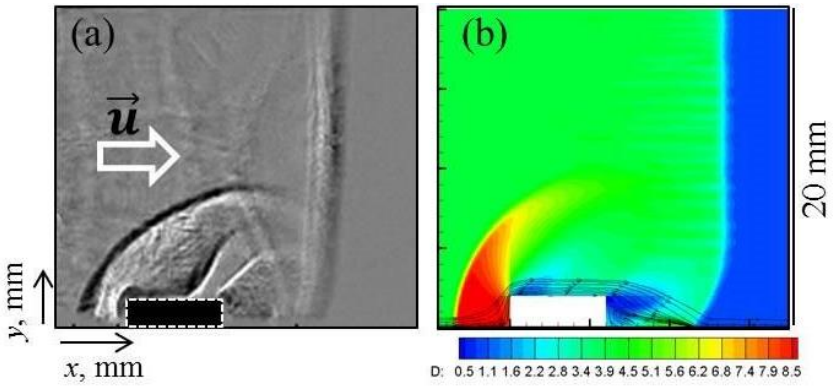

Fig. 3. Shock wave diffraction on an obstacle: shadow method (a), numerical calculation of density fields with streamlines (b); flow velocity u = 800±20 m/s

Comparative analysis of the numerical calculation results of gas-dynamic parameters and experimental frames from high-speed imaging (shadow and infrared) showed a visual similarity of the main structural features of the studied flows.

Figure 3 shows two images of shock wave diffraction on an obstacle. The high-velocity flow around the obstacle in the channel is defined by the inhomogeneous density field around the streamlined insert (Fig. 3 right). The area near the windward wall of the obstacle is characterized by a high degree of density and temperature in the of flow deceleration zone.

The resulting quasi-two-dimensional flow around an obstacle can be split by a set of unsteady gas-dynamic structures: a bow shock, an oblique shock, a recirculation zone in the obstacle leeward region, an expanding wave fan (Prandtl–Meyer fan), reattachment shock, etc. [14]. In front of the reflected shock wave, a bifurcated structure is formed due to the propagation of the reflected shock along the boundary layer that developed behind the incident shock wave (Fig. 2) [15].

500-800 microseconds after the shock wave passage, the flow velocity in the channel decreases due to the arrival of the rarefaction wave and the flow configuration near the obstacle changes. The transonic flow mode is mainly accompanied by the low density area in front of the rectangular ledge and an oblique shock associated with the flow connection. In this mode, the shadow images show an oblique shock shifted to the obstacle trailing edge and a turbulent trail formed by a flow separation behind the obstacle.

The vortex zone of flow separation behind the obstacle is a zone of reduced gas density. Over time, the flow velocity behind the incident shock wave decreases, the flow is turbulized. The results of numerical calculation in the transonic flow mode demonstrate the presence of a rarefaction region where the current lines are curved with the formation of an oblique shock associated with the flow connection (Fig. 2,3).

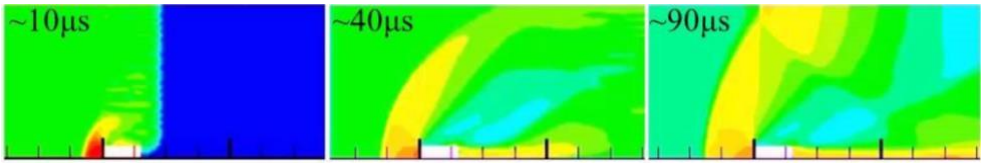

Fig. 4. Numerical simulation of the flow temperature field: frame-by-frame instantaneous distribution $u = 790 \pm 20\ m/s$ behind the shock wave $M = 3.2$

3.3 Thermography

There is a sharp decrease in velocity from its maximum value to zero on the surface of the walls of the shock tube in the boundary layer behind the plane shock wave [16]. The velocities gradient of the decelerating gas across the boundary layer leads to the appearance of significant friction forces, their work is converted into heat. Large thermophysical parameters changes in the boundary layer lead to heating of the streamlined surfaces: upper and lower walls, obstacle walls, side walls (glass). A change in the gas temperature at the shock wave front and in the supersonic flow behind it leads to a corresponding change in heat fluxes times on streamlined surfaces. Thus, in the area near the edge of the obstacle, successive changes in the flow configurations and interaction in the boundary layers implement a set of thermal fields on the channel walls corresponding to the interaction of the unsteady flow with the obstacle and the evolution of the near-surface satellite flow on them (Fig. 5).).

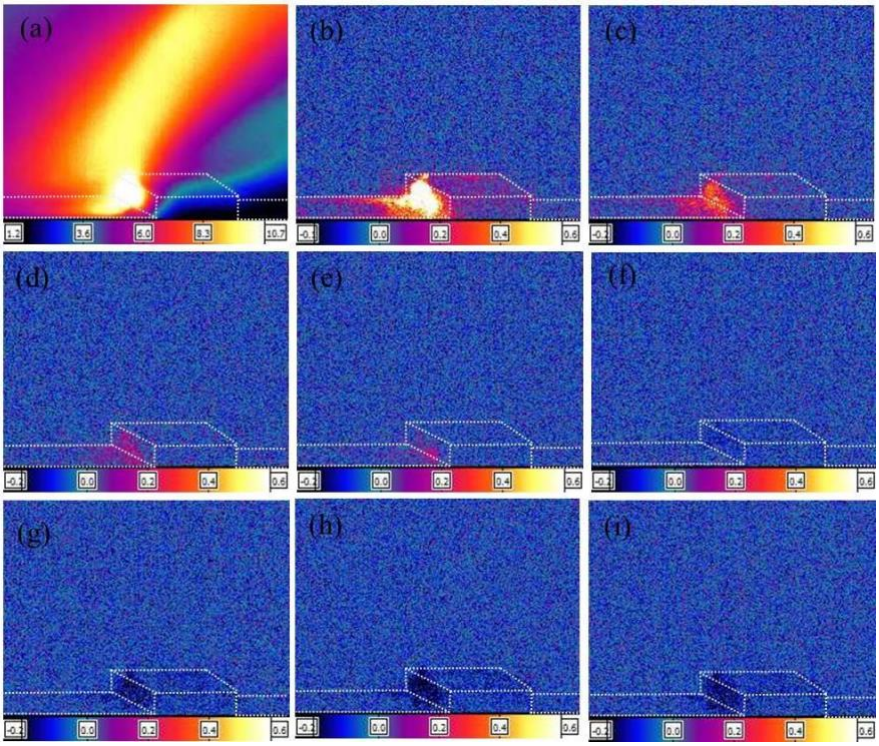

Fig. 5. The evolution of thermal fields $M = 4{,}0$ after the passage of the shock [windward side; $\tau_{EXP} = 1000\ \mu s$]: a) τ=0 ms; b) τ=2 ms; c) τ=4 ms; d) τ=6 ms; e) τ=12 ms; f) τ=16 ms; g) τ=22 ms; h) τ=26 ms; i) τ=32 ms

The thermodynamic balance on the wall consists of the ratio of the processes involved in heat exchange: unsteady thermal conductivity into the streamlined wall surfaces, convective

heat transfer between the boundary layer and the wall, as well as a complex configuration of radiant heat exchange between the flow and the streamlined surface. The heat flow formed in the channel boundary layer on the inner wall penetrates into a sufficiently thin layer of the quartz wall of the window of the shock tube test section, marking a thermal trace that is visualized by a thermal imager.

The most intense regions of infrared radiation recorded from the channel surfaces after diffraction of a plane shock wave on an obstacle correlate with the corresponding regions in the temperature field numerical calculation (Fig. 4) [17]. The given color palette of thermographic images was automatically constructed from the data obtained in the experiment by the Reveal-IR processor soft. Conventional units of the color scale reflect the dimensionless intensity of thermal radiation on thermograms, taking into account the subtracted background.

The integral map of heat fluxes during the exposure time of the first frame reflects the distribution of temperature fields in the areas of surface flow. During this time (τ= 2 ms) (Fig. 5 a) in the area in front of the upstream wall of the obstacle, the reflected shock wave moves upstream at a speed depending on the speed of the incoming (satellite) flow. The thermal imager registers the heated (during integration time) areas of the quartz wall in the near-surface boundary layer. The end of a supersonic satellite flow by a contact surface is visualized by a sharp decrease in the radiation level in the survey zone (Fig. 5 b-e). The flow mode for the next few milliseconds is characterized by radiation of a small area of the obstacle upstream wall, heated by a reflected outgoing jump, as well as a narrow strip of the lower channel wall in front of the obstacle.

The rarefaction wave significantly reduces the flow temperature. After τ ≈ 14 ms, a complete decrease in the intensity of thermal radiation from the previously heated obstacle surface area to the background level and below is recorded (Fig. 5 f). Later, the upwind side of the obstacle cools down to a time of τ ≈ 20-25 ms (Fig. 5 g–i), followed by a slow recovery to the initial thermal state at times of τ ≈ 40 ms.

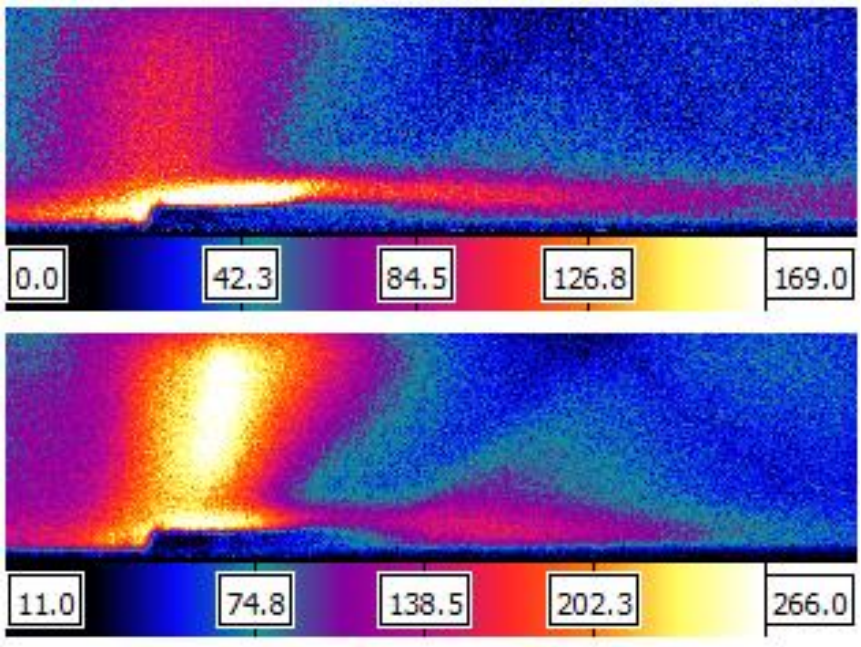

Fig. 6. Thermographic images of the thermal fields maps behind the backward step $[\tau_{EXP} = 500\ \mu s]$ (upper $M = 2{,}6$; lower $M = 3{,}0$)

Figure 6 shows larger scale thermographic images of the two-dimensional thermal fields, taken at an angle of α≈25° relative to the channel, with a shorter camera exposure time (flow from left to right). At the incident wave Mach number change, the distribution of thermal fields undergoes significant changes. The greatest intensity of radiation is observed in the

zones of complete flow deceleration. The effect of increased temperature values behind the incident shock wave on the channel walls above the obstacle leads to the formation and integral registration of a heated radiation region in the entire altitude of the channel.

Zones with reduced temperature and density are formed behind the obstacle (dark blue color) in the recirculation area, as well as in the fan of rarefaction waves, visualized on the downwind side of the insert.

Mach number increase (Fig. 6 lower image) leads to an increase in the values of the recorded thermal radiation, practically, on the entire panoramic heat map in the registration zone. The local radiation maxima of the heated channel wall become comparable to the radiation at the upwind obstacle side, where the peak radiation value had been previously recorded.

In order to separate heat fluxes from the far-off chamber window heated by the near-surface flow (separately from the nearby window), experiments were carried out to register the flow at a large viewing angle relative to the channel axis ($\alpha \approx 40°$-$45°$ in the horizontal plane). Figure 7 presents two similar images of heat fluxes separated horizontally, in accordance with the two inner surfaces of the heated windows of the test chamber.

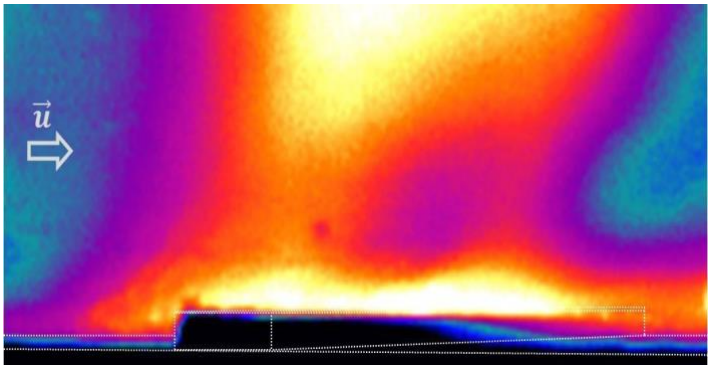

Fig. 7. Thermographic image of the thermal fields maps behind the backward step $M = 3{,}7$ $[\tau_{EXP} = 500\ \mu s]$

Consequently, it is shown that thermographic infrared imaging of the thermal fields of the inner surfaces of transparent quartz glasses makes it possible to visualize elements of gas–dynamic structures of unsteady flow adjacent to the windows, hery - after diffraction of a plane shock wave in a channel on a rectangular obstacle (Fig. 7).

4. Conclusion

An experimental study of the thermal fields from the shock tube test chamber surfaces, heated by a high-speed flow after the shock wave diffraction on the rectangular obstacle and the flow evolution was carried out. The heating and cooling of the test chamber walls streamlined by a high–speed flow are visualized using the Telops FAST M200 high-speed infrared camera (operating range 1.5 - 5.1 microns) through quartz windows transparent to infrared radiation. The thermal fields visualization results are compared to the shadow images of high-speed gas flow shooting, as well as to the data obtained by two–dimensional numerical simulation of the unsteady gas-dynamic process of shock wave M=2.0-4.5 diffraction. It is shown that the thermal fields' visualization of a complex unsteady gas-dynamic flow is supplemental to the inhomogeneous heating of the channel walls, including the inner surface of the side windows.

Acknowledgments

This work was supported by the Russian Foundation for Basic Research 23-19-0096.

References

1. **S.S. Kutateladze, A.I. Leontev** Heat Transfer, Mass Transfer, and Friction in Turbulent Boundary Layers, (Hemisphere Publishing Corp., New York, 1990), pp. 45-56.
2. **Frazier C., Lamnaouer M., Divo E., Kassab A., Petersen E.** Effect of wall heat transfer on shock-tube test temperature at long times // Shock Waves. 2011. V. 21. № 1. P. 1–17.
3. **Volpiani P., Larsson J., Bernardini M.** Effects of a nonadiabatic wall on supersonic shock/boundary-layer interactions // Physical review fluids. 2018. V. 3 083401.
4. **Nakamura H.** Spatio-temporal measurement of convective heat transfer using infrared thermography. Heat Transfer - Theoretical Analysis, Experimental Investigations and Industrial Systems. InTech, 2011.
5. **Znamenskaya I.** Methods for panoramic visualization and digital analysis of thermophysical flow fields // Scientific visualization. 2021. 13(3) P. 125–158.
6. **Settles G., Hargather M.** A review of recent developments in schlieren and shadowgraph techniques // Measurement Science and Technology. 2017. V. 28. № 4.
7. **V. Vavilov** Infrared thermography and thermal control, (ID Spectrum, Moscow, 2009), pp. 45-544.
8. **Knauss H., Roediger T., Bountin A.** Novel Sensor for Fast Heat Flux Measurements. J. Spacecraft and Rockets. 2009. V. 462. № 2.
9. **I.A. Znamenskaya, E.Yu. Koroteeva, M.I. Muratov et al.** Registration of Nonstationary Heat Flux Dynamics in Shock Tubes Using High-Speed Thermography // Moscow University Physics Bulletin. 6, pp. 914-921 (2023).
10. **Running C., Rataczak J., Zaccara M., Cardone G., Juliano T**. A wrap-film technique for infrared thermography heat-transfer measurements in high-speed wind tunnels // Experimental Thermal and Fluid Science. 2022. V 135.
11. **Cardone G., Zaccara M., Edelman J.** A general procedure for infrared thermography heat transfer measurements in hypersonic wind tunnels // International Journal of Heat and Mass Transfer. 2020. V 163. 120419.
12. **Carlomagno G.M., Cardone G.** Infrared thermography for convective heat transfer measurements // Exp. Fluids. 2010. V. 49. № 6. P. 1187–1218.
13. **Lutsky A.E., Kudryashow I.Y., Khankhasaeva Y.V.** Numerical simulation of the influence of energy deposition on the base flow // Mathematical Models and Computer Simulations. 2016. V. 8. P. 207–218.
14. **Znamenskaya I.A., Dolbnya D.I., Ivanov I.E., Kuli-zade T.A., Sysoev N.N.** Pulse volume discharge behind shock wave in channel flow with obstacle // Acta Astronautica. 2022. V. 195. P. 493–501.
15. **Kleine H., Lyakhov V.N., Gvozdeva L.G., Grönig H.** Bifurcation of a reflected shock wave in a shock tube. Berlin Heidelberg: Springer, 1992.
16. **H. Schlichting** Grenzschichttheorie, (Braun Verlag, Karlsruhe, 1965)
17. **I.A. Znamenskaya, E.A. Karnozova, T.A. Kuli-zade** The discharge heated channel region visualization based on thermal imaging registration // Scientific Visualization. 14 (2022)